SCIENTIFIC REPORTS

OPEN

Direct Photochemical C–H Carboxylation of Aromatic Diamines with CO₂ under Electron-Donor- and Base-free Conditions

Takeshi Matsumoto[1,2], Daiki Uchijo[1], Takuji Koike[1], Ryoya Namiki[1] & Ho-Chol Chang[1]

We report the photochemical carboxylation of *o*-phenylenedimamine in the absence of a base and an electron donor under an atmosphere of CO_2, which afforded 2,3-diaminobenzoic acid (DBA) in 28% synthetic yield and 0.22% quantum yield (Φ(%)). The synthetic yield of DBA in this reaction increased to 58% (Φ(%) = 0.47) in the presence of Fe(II). The photochemical reaction described in this work provides an effective strategy to use light as the driving force for the direct carboxylation of organic molecules by CO_2.

Owing to the ever-increasing desire to use carbon dioxide (CO_2) as an C_1 feedstock[1–6], the development of heterogeneous[5,7] and homogeneous[4,8–21] catalysts for the transformation of CO_2 into reduced C_1 compounds[8,9,17–21] or CO_2-containing organic compounds has received considerable attention[10–16]. In the former case, several thermal hydrogenation[8,9], electro-[17–19], and photo-catalytic systems[17,18,20,21] that produce reduced C_1 chemicals, e.g., CH_3OH[22–24], CO[25–30], HCO_2H[31–33], and HCO_2^-[34–36] have been investigated. In the latter case, carboxylic acids are formed, which represent a central motif in a variety of synthetically important chemicals[37–50].

Recently, the direct carboxylation of aryl rings has garnered considerable attention. For example, Nolan *et al.* reported the [M(IPr)(OH)] (M = Cu[I] or Au[I], IPr = 1.3-bis(diisopropyl)phenylimidazol-2-ylidene)-catalyzed carboxylation of halogenated benzene using KOH or CsOH as a base under an atmosphere of CO_2[42,43]. Iwasawa *et al.* also reported the Pd(OAc)₂-catalyzed photochemical carboxylation of aryl halides using [Ir(ppy)₂(dtbpy)][PF₆] (λ_{ex} = 425 nm; dtbpy = 4,4′-di-*tert*-butyl-2,2′-bipyridyl) as the photosensitizer and *i*Pr₂NEt as a sacrificial electron donor under CO_2[47]. In these reports, the presence of a base and/or electron donor is necessary for the thermal or photochemical reaction and the incorporation of CO_2. However, obtaining carboxylic acids directly from CO_2 in the absence of an electron donor and base would be more attractive in terms of atom- and step-economy.

We have recently reported the photochemical hydrogen evolution (PHE) from the Fe(II) complex [Fe^{II}(opda)₃][ClO₄]₂ (**1**; opda = *o*-phenylenediamine) (Fig. 1) under N₂[51], wherein opda acts as a photo-responsive proton/ electron pool that forms the partially oxidized *semi*-benzoquinodiimine (s-bqdi) or *o*-benzoquinodiimine ligands. The photochemical reaction of **1** under N₂ inspired us to investigate that under CO₂. Herein, we report the first example for a direct photochemical carboxylation of C–H bonds in aromatic diamines with CO₂ in the absence of an electron donor and base.

Results

Photochemical hydrogen evolution reactions from opda and 1 under N₂ or CO₂. The UV-Vis spectra of opda and **1** in THF under N₂ or CO₂ (Fig. 2a) exhibit absorption band at 298 nm, attributable to the $\pi\pi^*$ transition of opda and a transition with $\pi\pi^*$ character of **1**[51]. In the case of opda, spectral differences were not observed under N₂ or CO₂, indicating a negligible effect of the atmosphere on the electronic state. Even though the molar absorption coefficient of **1** changed slightly from N₂ to CO₂ (Fig. 2a), the similarity of the spectra and the fact that the same colorless crystals of **1** were obtained from THF/*n*-hexane under each atmosphere (Supplementary Fig. 1 and Supplementary Table 1) indicate that **1** is stable under both gases. When the solution was left to stand for 8 h under CO₂, there were virtually no UV-Vis spectral differences in both opda and **1** (Supplementary Fig. 2), demonstrating their stability in the dark. The ¹H NMR (THF-*d*₈) spectra of opda under

[1]Department of Applied Chemistry, Faculty of Science and Engineering, Chuo University, 1-13-27 Kasuga, Bunkyo-ku, Tokyo, 112-8551, Japan. [2]Precursory Research for Embryonic Science and Technology (PRESTO), Japan Science and Technology Agency (JST), 4-1-8 Honcho, Kawaguchi, Saitama, 332-0012, Japan. Correspondence and requests for materials should be addressed to H.-C.C. (email: chang@kc.chuo-u.ac.jp)
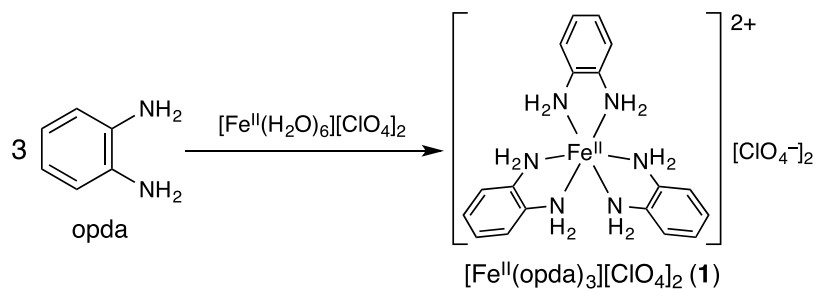
Figure 1. Synthesis of **1** from opda and $[Fe^{II}(H_2O)_6][ClO_4]_2$.

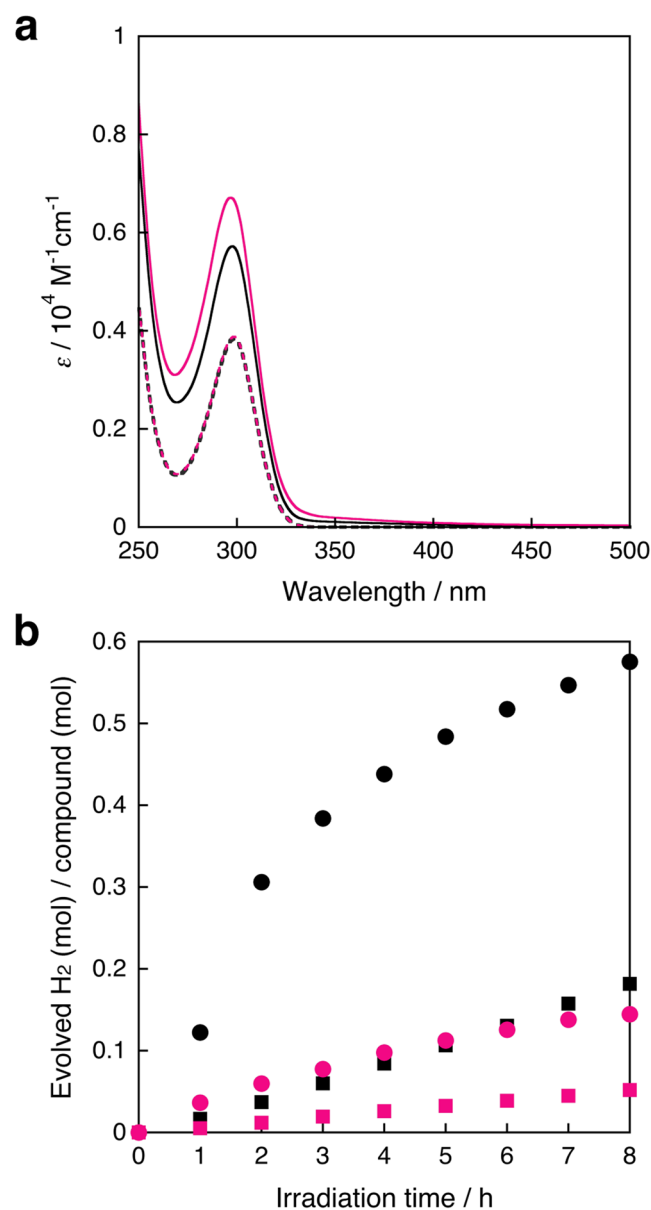**Figure 2.** (**a**) UV-Vis spectra of opda (6.0×10^{-3} M) under N_2 (···) or CO_2 (· ·), and **1** (2.0×10^{-3} M) under N_2 (—) or CO_2 (—) in THF at room temperature. (**b**) Time-course plots of the amount of photochemically evolved hydrogen from a) opda (6.0×10^{-3} M; 1.2×10^{-5} mol/4 mL; $\lambda_{ex} = 300 \pm 10$ nm; 63.5–66.9 mW) under N_2 (■) or CO_2 (■), and **1** (2.0×10^{-3} M; 8.0×10^{-6} mol/4 mL; $\lambda_{ex} = 300 \pm 10$ nm; 63.9–66.9 mW) under N_2 (●) or CO_2 (●) in THF.
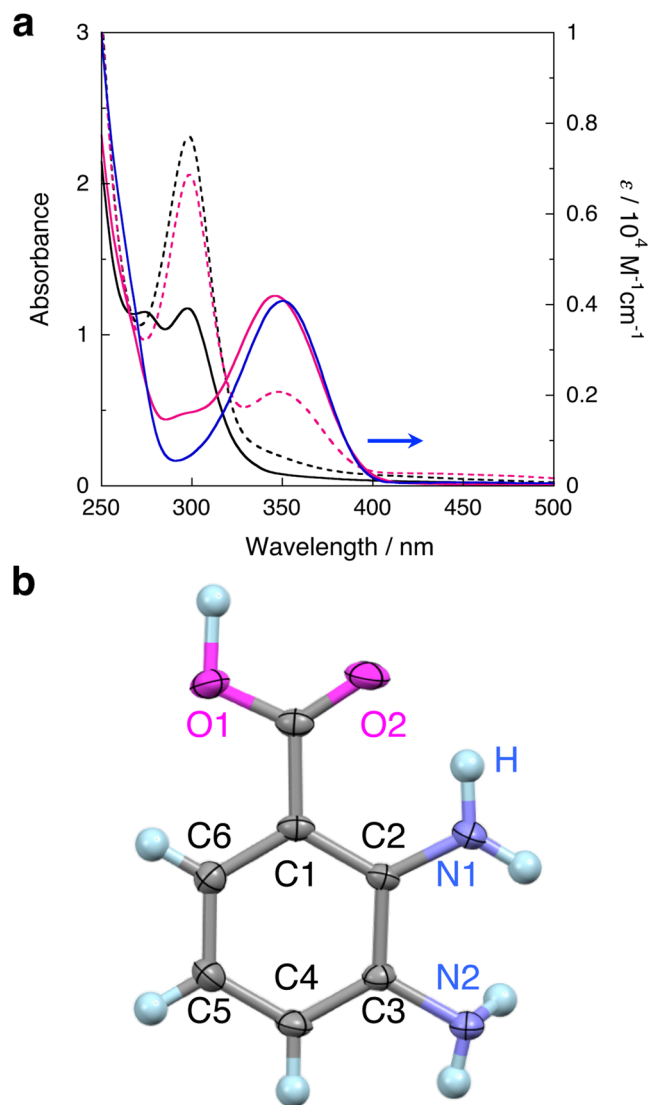
Figure 3. (**a**)UV-Vis spectra of opda (6.0×10^{-3} M) after irradiation ($\lambda_{ex} = 300 \pm 10$ nm; 63.9–66.9 mW) under CO_2 (· · ·) or N_2 (···), and those of **1** (2.0×10^{-3} M) under CO_2 (——) or N_2 (—) in THF (8 h; room temperature), together with spectrum of commercial DBA (——). (**b**) Crystal structure of DBA (unit A); atomic displacement parameters set to 50% probability; color-code: blue = N, gray = C, magenta = O, and light blue = H; hydrogen atoms are depicted in ball-and-stick mode for clarity.

N_2 or CO_2 (Supplementary Fig. 3) show characteristic signals at 6.42, 6.50, and 3.80 ppm, assignable to aromatic C–H and N–H protons. On the other hand, the spectra of **1** under N_2 or CO_2 (Supplementary Fig. 3) did not show any clear signals, reflecting its paramagnetic nature[51]. Aromatic amines afford carbamic acids or benzimidazol-2-one from the reaction with CO_2 under basic conditions[52,53] or in the presence of catalysts[54–56]. However, such products could not be detected under these dark conditions.

When a THF solution of opda was irradiated with UV light ($\lambda_{ex} = 300 \pm 10$ nm) under N_2, PHE was observed with an apparent quantum yield of $\Phi_{H2@N2}(\%) = 1.28 \times 10^{-3}$ (8 h) (Fig. 2b). Contrastively, the amount of evolved hydrogen under CO_2 decreased by one third under N_2 ($\Phi_{H2@CO2}(\%) = 4.16 \times 10^{-4}$) (8 h). Under these conditions, a THF solution of **1** also showed PHE with $\Phi_{H2@N2}(\%) = 0.0138$ (8 h) and $\Phi_{H2@CO2}(\%) = 3.56 \times 10^{-3}$ (8 h) (Fig. 2b). The observed inhibitions of the PHE under CO_2 clearly suggest an alternative photochemical process under CO_2 compared to that under N_2.

Direct photochemical carboxylation of aromatic diamines with CO_2 by opda and 1.

The UV-Vis spectra of opda and **1** after photo-irradiation (8 h) under CO_2 showed new absorption band at 347 nm (Fig. 3a). It is noteworthy that the new band was observed only when the photoreaction took place under CO_2 (Supplementary Fig. 2). Interestingly, the absorbance of the new bands was significantly increased for **1** relative to opda, which confirms the promoting effect of the Fe(II) ion in **1**. The ^{1}H NMR (CD_3CN) spectrum after the photoreaction of opda under CO_2 (Supplementary Fig. 4) exhibits two sets of doublets at 6.82 and 7.30 ppm, as
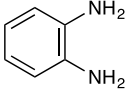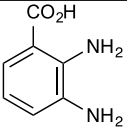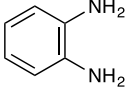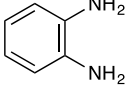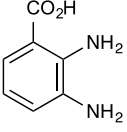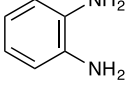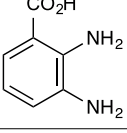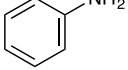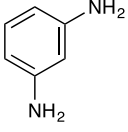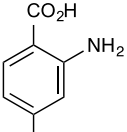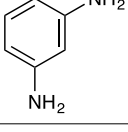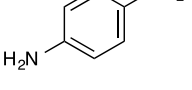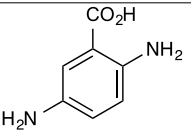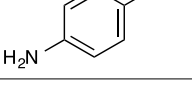
Run	Substrate	Metal	λ_{max} (nm)	λ_{ex} (nm)	Product	Yield(%)[b]	Φ(%)[c]
1[d]	(o-phenylenediamine)	Fe(II)	298	300 ± 10	(2,3-diaminobenzoic acid)	54.1	0.44
2[d]	(o-phenylenediamine)	Fe(II)	298	—	N.D.[e]	—[g]	—[g]
3	(o-phenylenediamine)	Fe(II)	298	300 ± 10	(2,3-diaminobenzoic acid)	58.0	0.47
4	(o-phenylenediamine)	—	298	300 ± 10	(2,3-diaminobenzoic acid)	27.5	0.22
5	(aniline)	Fe(II)	291	289 ± 10	N.D.[e]	—[g]	—[g]
6	(m-phenylenediamine)	—	298	300 ± 10	(carboxylated diamine)	trace	—[g]
7	(m-phenylenediamine)	Fe(II)	—[f]	—[f]	—[f]	—[f]	—[f]
8	(p-phenylenediamine)	—	324	300 ± 10	(carboxylated diamine)	trace	—[g]
9	(p-phenylenediamine)	Fe(II)	—[f]	—[f]	—[f]	—[f]	—[f]

Table 1. Results of the photo-irradiation of aromatic amines under CO_2[a]. [a]Reaction time: 8 h; light power: 63.5–66.9 mW ($\lambda_{ex} = 300 \pm 10$ nm) and 55.1 mW (289 ± 10 nm). [b]Estimated based on the amounts of used aromatic amines and absorbance of the products. [c]Apparent quantum yield (%). [d]The *ex-situ*-prepared Fe complex was used. [e]Not detected. [f]The reaction was not investigated due to the formation of precipitates after mixing $[Fe^{II}(H_2O)_6][ClO_4]_2$ and 3 eq. of the substrates. [g]Not estimated.

well as a triplet at 6.51 ppm, suggesting the formation of a 1,2,3-trisubstituted benzene. A similar spectrum was observed after the photoreaction of **1** under identical conditions (Supplementary Fig. 4). X-ray diffraction analysis of the pale yellow crystals of the product unambiguously identified 2,3-diaminobenzoic acid (DBA) (Fig. 3b and Supplementary Fig. 5, Supplementary Tables 2 and 3)[57,58]. Interestingly, one *ortho* C–H bond relative to an amino group was carboxylated. The similarity between the UV-Vis and ^{1}H NMR spectra of commercial DBA and the photochemical products of opda or **1** (Fig. 3a and Supplementary Fig. 6) indicates that DBA is the main product, while the isomer, i.e., 3,4-diaminobenzoic acid, was not obtained in detectable amounts. Based on the molar absorption coefficient of DBA ($\varepsilon = 4{,}041$ M^{-1} cm^{-1}) at 347 nm (Fig. 3a), the photochemical reaction of **1**, prepared *in-situ* by mixing $[Fe^{II}(H_2O)_6][ClO_4]_2$ and 3 eq. of opda (run 3 in Table 1), afforded DBA in 58.0% ($\Phi(\%) = 0.47$), which is comparable to that for *ex-situ*-prepared **1** (54.1%; $\Phi(\%) = 0.44$) (Supplementary Fig. 7 and run 1 in Table 1). On the other hand, the photo-irradiation of a THF solution of opda afforded DBA in 27.5% ($\Phi(\%) = 0.22$) (Fig. 3a and run 4 in Table 1).

A reaction mechanism for the photochemical carboxylation. To get insight into the underlying reaction mechanisms, we subsequently carried out the photoreaction with aniline and Fe(II) under CO_2. However, the UV-Vis spectrum showed no significant changes (Supplementary Fig. 8 and run 5 in Table 1). The
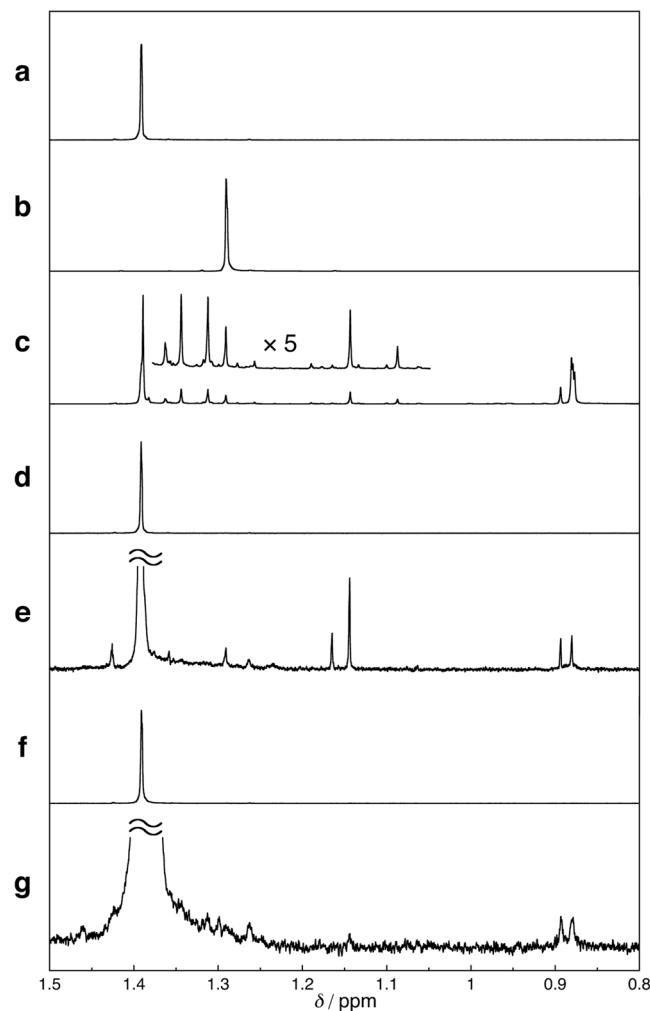
Figure 4. ^1H NMR (THF-d_8, 500 MHz) spectra of (**a**) t-BuSH, (**b**) t-Bu$_2$S$_2$, (**c**) t-Bu$_2$S$_2$ after photo-irradiation ($\lambda_{ex} = 300 \pm 10$ nm; 64.5 mW; 3 h), (**d**) t-BuSH with opda, (**e**) t-BuSH after photoirradiation ($\lambda_{ex} = 300 \pm 10$ nm; 64.2 mW; 3 h) in the presence of opda, (**f**) t-BuSH with **1**, and (**g**) t-BuSH after photo-irradiation ($\lambda_{ex} = 300 \pm 10$ nm; 64.5 mW; 3 h) in the presence of **1**, in THF-d_8 under CO$_2$.

inertness of aniline prompted us to use m- (mpda) and p-phenylenediamine (ppda)[59,60]. The photo-irradiations ($\lambda_{ex} = 300 \pm 10$ nm) of mpda or ppda resulted in the emergence of new absorbances at 360 nm and 400 and 450 nm, respectively (Supplementary Fig. 9, runs 6 and 8 in Table 1). Curiously, the absorbances of mpda and ppda were observed even after irradiation, suggesting their poor reactivity (Supplementary Fig. 9). ESI-MS spectra showed signals (m/z 151.05) for the carboxylated products in the crude reaction mixture (Supplementary Figs 10a and 11a). The newly emerged ^1H NMR signals of the carboxylated products were assigned to 2,4- and 2,5-diaminobenzoic acids (Supplementary Figs 10b and 11b). Conversely, the treatment of mpda or ppda with Fe(II) afforded white precipitates, probably due to the formation of coordination polymers (runs 7 and 9 in Table 1)[61,62].

Given the atmosphere-dependent photoreactions of opda and **1**, we focused our attention on their excited states. The emission spectra ($\lambda_{ex} = 300$ nm) of opda and **1** in THF under N$_2$ or CO$_2$ showed the emission bands at 350 nm, assignable to emissions from $\pi\pi^*$ of opda or $\pi\pi^*$ included excited state of **1** (Supplementary Fig. 12). In the excitation spectra of opda and **1** under N$_2$ or CO$_2$ ($\lambda_{obs} = 350$ nm), the bands were observed at 298 nm, suggesting radiative deactivation pathways for the photoreactions under N$_2$ and CO$_2$ (Supplementary Fig. 13).

Subsequently, we attempted to identify the active species by trapping experiments. It was previously reported that 2-methylpropane-2-thiol (t-BuSH) can act as a hydrogen (H) radical scavenger forming di-$tert$-butyl disulfide (t-Bu$_2$S$_2$)[63,64]. The detection of t-Bu$_2$S$_2$ among the photochemical reaction products of opda and **1** revealed the H radical generation during the reaction (*vide infra*). The ^1H NMR spectra of t-BuSH and t-Bu$_2$S$_2$ under CO$_2$ (Fig. 4a,b, and Supplementary Fig. 14) showed singlets at 1.38 and 1.29 ppm, respectively. On the other hand, we found that the new signals emerged at 0.88, 0.89, and 1.19 ppm in the ^1H NMR spectrum of a THF-d_8 solution of t-Bu$_2$S$_2$ after photo-irradiation ($\lambda_{ex} = 300 \pm 10$ nm), which demonstrates the photoreactivity of t-Bu$_2$S$_2$ (Fig. 4c)[63]. These resonances are thus indicative of the *in-situ* formation of t-Bu$_2$S$_2$. A mixture of opda/t-BuSH displayed a ^1H NMR spectrum similar to those of pure t-BuSH and opda (Fig. 4d and Supplementary Fig. 14),
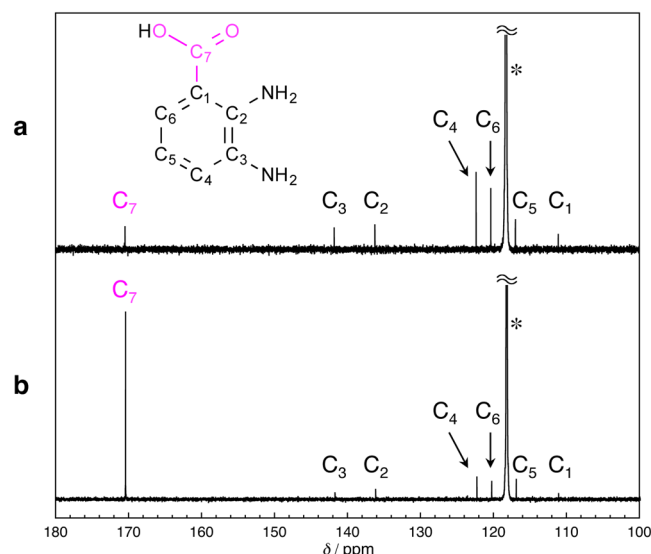
Figure 5. ^{13}C NMR (CD$_3$CN, 126 MHz) spectra of the photochemical product ($\lambda_{ex} = 300 \pm 10$ nm) of **1** under (**a**) CO$_2$ and (**b**) $^{13}CO_2$ in THF at room temperature. The symbol "*" indicates the ^{13}C NMR signals of CD$_3$CN.
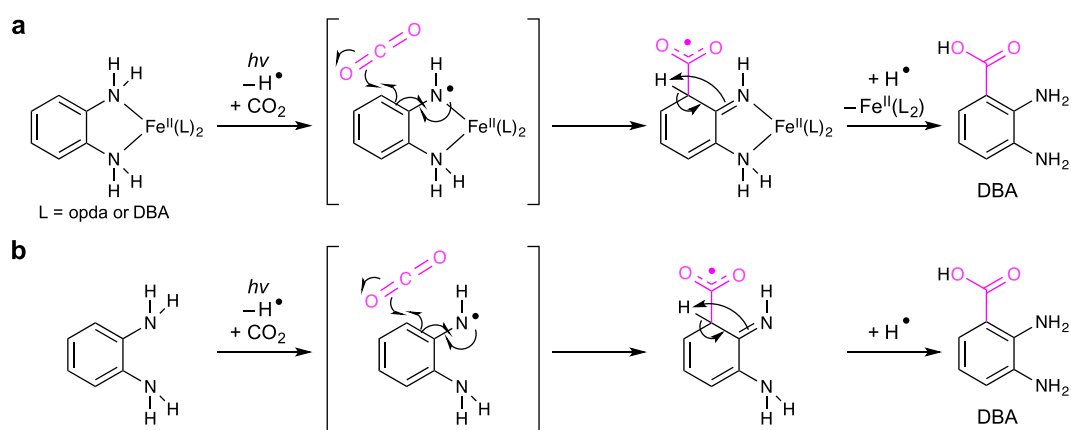

Figure 6. Plausible reaction mechanisms for the photo-induced direct carboxylation of opda in the (**a**) presence and (**b**) absence of Fe(II).

suggesting negligible interactions in the ground state. After photo-irradiation, new singlets emerged at 0.88, 0.89, and 1.19 ppm (Fig. 4e), and these peaks are identical to those of the photochemical products derived from *t*-Bu$_2$S$_2$ (Fig. 4c), suggesting the formation of *t*-Bu$_2$S$_2$ during the photochemical reaction. The ^1H NMR spectrum of a mixture of **1**/*t*-BuSH showed no significant interaction in the ground state (Fig. 4f), whereas new singlets emerged at 0.88 and 4.61 ppm after photo-irradiation (Fig. 4g and Supplementary Fig. 14). These peaks are comparable to those of the photochemical products of opda/*t*-BuSH mixture (Fig. 4e), suggesting the formation of *t*-Bu$_2$S$_2$ from **1**/*t*-BuSH. Based on these results, it should be feasible to consider a reaction pathway involving the H radical generation for the photoreaction of opda and **1** under CO$_2$. The lower amount of photochemically generated H$_2$ from them under CO$_2$ than N$_2$ thus most likely reflects the incorporation of the generated H radicals in the DBA skeleton.

Finally, to shed more light on the reaction mechanism, we compared the ^{13}C NMR (CD$_3$CN) spectra of the reaction product of **1** under CO$_2$ or $^{13}CO_2$. In the ^{13}C NMR spectrum of the photochemically-produced DBA from **1** under CO$_2$, the resonance derived from the carboxyl carbon was observed at 170.5 ppm (Fig. 5a). In the case of the photoreaction under $^{13}CO_2$, the peak intensity of the carboxyl carbon clearly increased, suggesting that the carboxyl moiety in DBA originates from CO$_2$ (Fig. 5b)[14,65].

Figure 6 depicts plausible mechanisms for the photochemical carboxylation of opda and **1**. Given the aforementioned results, the photo-irradiation induces the generations of H and aminyl radical intermediates. The later then form a C–C bond with CO$_2$ *via* the delocalization of the unpaired electron, thus forming the carboxyl radical intermediate[66]. Subsequently, the methine proton transferrs to the imino nitrogen, whereby the aromatic stabilization could act as driving force forming a 2,3-diaminobenzoic radical species. The reaction of the intermediate

with a H radical might finally yield DBA. The role of the Fe(II) ion in this reaction should be worth investigating in detail, as it is highly plausible that the Fe(II) center perturbs the N–H moiety in opda favorably[64,67–71].

Discussion

In this paper, we demonstrated a direct photochemical C–H carboxylation of aromatic diamines with CO_2. Although this reaction is not catalytic, it represents the first example of atom- and step-economic direct carboxylation of a C–H bond in benzene rings in the absence of any potentially reactive electron donor and base. The promotion of this reaction by Fe(II) could be achieved using opda ligand, indicating the potential of nonprecious metal ions to accelerate or catalyze the reaction. Further efforts to gain an in-depth understanding of the mechanism and to expand the scope of the reaction by using a wider range of aromatic polyamines, nonprecious metal ions, excitation wavelengths, and catalytic protocols are currently in progress.

Methods

General procedures.   All synthetic operations were performed under N_2 or CO_2 using standard Schlenk-line techniques. The ligand opda was purchased from Wako Pure Chemical Industries (Japan), while *p*-phenylenediamine (ppda) was obtained from Sigma-Aldrich, and *m*-phenylenediamine (mpda), was procured from Tokyo Chemical Industry Co., Ltd. (Japan). 2,3-Diaminobenzoic acid (DBA) was purchased from Combi-blocks (USA) and used after recrystallization from H_2O. Dehydrated THF, THF-d_8, CD_3CN, and silica gel (60 N) were purchased from Kanto Chemical Co. Inc. (Japan). MeOH, CH_3CN, and emission analysis grade THF were obtained from Nacalai Tesque, Inc. (Japan). N_2, CO_2, and $^{13}CO_2$ were purchased from Kotobuki Sangyo Co. Ltd. (Japan). Prior to use, THF was degassed by at least five freeze-pump-thaw cycles, followed by N_2 or CO_2 sparging for 20 min, and subsequent dehydration over molecular sieves (4 Å, MS4A), which were purchased from Wako Pure Chemical Industries (Japan) and activated by heating under high vacuum. Complex $[Fe^{II}(opda)_3][ClO_4]_2$ (**1**) was prepared according to a previously reported procedure[51]. Caution! Although we did not experience any difficulties manipulating perchlorate salts, these should be regarded as potentially explosive and therefore require handled with the utmost care.

UV-Vis-NIR spectra were recorded on a HITACHI U-4100 spectrophotometer at room temperature (25 °C). IR spectra were recorded on a Thermo Nicolet 6700 FT-IR spectrometer by attenuated total reflection (ATR) method. ^1H and ^{13}C NMR (500 and 126 MHz) spectra were recorded on a JEOL EX-500 (and A-500) spectrometer using CD_3CN or THF-d_8. Elemental analyses were carried out on a Perkin-Elmer 2400 II CHN analyzer. Electrospray ionization mass spectra (ESI-MS) were performed at the Global Facility Center at Hokkaido University. Emission and excitation spectra were recorded on a Horiba FluoroMax-4 spectrophotometer at room temperature (25 °C).

Preparation of the solutions used for the reactions under atmospheres of N_2 or CO_2 (in the dark or under irradiation).   The sample solutions for reactions under N_2 or CO_2 were prepared under the respective atmospheres. A colorless THF solution (2.0 mM) of *ex-situ*-prepared $[Fe^{II}(opda)_3][ClO_4]_2$ was obtained from dissolving $[Fe^{II}(opda)_3][ClO_4]_2$ (6.51 mg, 1.0×10^{-5} mol) in THF (5 mL). On the other hand, *in-situ*-prepared $[Fe^{II}(opda)_3][ClO_4]_2$ was obtained from the treatment of $[Fe^{II}(H_2O)_6][ClO_4]_2$ (3.63 mg, 1.0×10^{-5} mol) with opda (3.24 mg, 3.0×10^{-5} mol) in THF (5 mL). In a similar manner, a colorless THF solution of a mixture of $[Fe^{II}(H_2O)_6][ClO_4]_2$ and aniline was prepared using aniline (2.73 µL, 3.0×10^{-3} mol) instead of opda. THF solutions (6 mM) of Fe^{II}-free opda, aniline, mpda, or ppda were prepared by dissolving opda (3.24 mg, 3.0×10^{-5} mol), aniline (2.73 µL, 3.0×10^{-3} mol), mpda (3.24 mg, 3.0×10^{-5} mol), or ppda (3.24 mg, 3.0×10^{-5} mol) in THF (5 mL).

To investigate the reactivity under photo-irradiation, 0.4 mL of the respective sample solutions were transferred into a N_2- or CO_2-filled 1 mm quartz cell and the UV-Vis spectrum of the initial state was measured. The remaining 4 mL of the sample solution were then transferred into a custom-made Schlenk-flask-equipped quartz tube (volume: 164 mL). After exposing this apparatus for 8 h to photo-irradiation, 0.4 mL of the sample solution were withdrawn and transferred into a N_2- or CO_2-filled 1 mm quartz cell in order to measure the UV-Vis spectrum. In order to examine the reactivity in the dark, 0.4 mL of the solution were transferred into a N_2- or CO_2-filled 1 mm quartz cell and the UV-Vis spectrum of the initial state was measured. After allowing the sample solutions to stand for 8 h, in the dark, the spectral measurements were recorded again.

Photochemical hydrogen evolution.   For the photochemical hydrogen-evolution reaction (HER), the aforementioned Schlenk-flask-equipped quartz tube (volume: 164 mL) and THF solutions (4 mL) were used. The light source for the photochemical reactions was a 200 W Hg-Xe lamp (LC-8, Hamamatsu Photonics K.K.), and the intensity of the light was measured by using a power meter (Nova, Ophir Optronics Ltd.) and a thermo-pile sensor (3 A, Ophir Optronics Ltd.) prior to photo-irradiation experiments. Gas chromatographic analyses were conducted using a Shimadzu gas chromatograph (GC-2014) equipped with a thermal conductivity detector (TCD), a column filled with 5 Å molecular sieves, and Ar as the carrier gas (15.0 mL/min). The oven temperature was maintained at 100 °C, while the column and detector temperatures were set to 70 °C and 200 °C, respectively. Before the photo-irradiation experiments, a gas sample (0.3 mL) was collected from the headspace using a gas-tight syringe (Tokyo Garasu Kikai Co. Ltd) and analyzed by GC to confirm the successful N_2 or CO_2 purge. The samples were then exposed to irradiation in a water bath at room temperature. During the reaction, gas samples (0.3 mL) were collected from the headspace in order to determine the amount of H_2 evolved as a function of the irradiation time.

Purification of DBA after the photoreactions. After the reactions in the dark or upon photo-irradiation, as well as measurements of UV-Vis spectra of the samples after the reaction, all THF solutions were transferred into a Schlenk flask and THF was removed under reduced pressure. After measuring of the ^{1}H NMR and ESI-MS spectra, the reaction mixtures were purified by flash column chromatography (Isolera One ACI™ Spektra, Biotage Co. Ltd.) on silica gel (60 N; Kanto Chemical Co. Inc.; eluent: $CH_3CN:MeOH = 9:1$ then 0:10). The photochemical products of $[Fe^{II}(opda)_3][ClO_4]_2$ or Fe^{II}-free opda were collected and dried *in vacuo*. The formation of DBA was confirmed by recording the ^{1}H NMR spectra in CD_3CN. Colorless single crystals of DBA suitable an X-ray crystallographic analysis were obtained from a recrystallization from THF/*n*-hexane.

Calculation of the quantum yields (Φ%). The THF solutions of the samples, except for those of aniline and a mixture of aniline and $[Fe^{II}(H_2O)_6][ClO_4]_2$, were exposed to photo-irradiation ($\lambda_{ex} = 300 \pm 10$ nm) from a Hg-Xe lamp equipped with the LX0300 band pass filter (Asahi Spectra Inc.; $\lambda = 300 \pm 10$ nm; half bandwidth = 10.40 nm). The THF solutions of aniline and a mixture of aniline and $[Fe^{II}(H_2O)_6][ClO_4]_2$ were exposed to photo-irradiated ($\lambda_{ex} = 289 \pm 10$ nm) from a Hg-Xe lamp equipped with a CWL289 nm filter (OptoSigma Corporation, $\lambda = 289 \pm 10$ nm, half bandwidth = 10 nm). The amount of DBA formed in runs 1, 3, and 4 (Table 1) in the subsequent 8 h were used to calculate the apparent quantum yield (Φ) using Eq. 1.

$$\Phi = N_e/N_p = N_{DBA}/N_p \tag{1}$$

where, N_e refers to the number of reacted electrons, N_{DBA} to the number of molecules of DBA formed in the reaction, and N_p to the number of incident photons.

Data Availability
The X-ray crystallographic coordinates for the structure of DBA reported in this Article has been deposited at the Cambridge Crystallographic Data Centre (CCDC), under deposition number CCDC-1826028. These data can be obtained free of charge from The Cambridge Crystallographic Data Centre *via* http://www.ccdc.cam.ac.uk/data_request/cif.

References
1. Sakakura, T., Choi, J.-C. & Yasuda, H. Transformation of carbon dioxide. *Chem. Rev.* **107**, 2365–2387 (2007).
2. Mikkelsen, M., Jorgensen, M. & Krebs, F. C. The teraton challenge. A review of fixation and transformation of carbon dioxide. *Energy Environ. Sci.* **3**, 43–81 (2010).
3. Appel, A. M. *et al.* Frontiers, opportunities, and challenges in biochemical and chemical catalysis of CO₂ fixation. *Chem. Rev.* **113**, 6621–6658 (2013).
4. Cokoja, M., Bruckmeier, C., Rieger, B., Herrmann, W. A. & Kühn, F. E. Transformation of carbon dioxide with homogeneous transition-metal catalysts: A molecular solution to a global challenge? *Angew. Chem. Int. Ed.* **50**, 8510–8537 (2011).
5. Roy, S. C., Varghese, O. K., Paulose, M. & Grimes, C. A. Toward solar fuels: Photocatalytic conversion of carbon dioxide to hydrocarbons. *ACS Nano* **4**, 1259–1278 (2010).
6. Chang, Z., Jing, X., He, C., Liu, X. & Duan, C. Silver clusters as robust nodes and π-activation sites for the construction of heterogeneous catalysts for the cycloaddition of propargylamines. *ACS Catal.* **8**, 1384–1391 (2018).
7. Habisreutinger, S. N., Schmidt-Mende, L. & Stolarczyk, J. K. Photocatalytic reduction of CO₂ on TiO₂ and other semiconductors. *Angew. Chem. Int. Ed.* **52**, 7372–7408 (2013).
8. Artz, J. *et al.* Sustainable conversion of carbon dioxide: An integrated review of catalysis and life cycle assessment. *Chem. Rev.* **118**, 434–504 (2018).
9. Grice, K. A. Carbon dioxide reduction with homogenous early transition metal complexes: Opportunities and challenges for developing CO₂ catalysis. *Coord. Chem. Rev.* **336**, 78–95 (2017).
10. Maeda, C., Miyazaki, Y. & Ema, T. Recent progress in catalytic conversions of carbon dioxide. *Catal. Sci. Technol.* **4**, 1482–1497 (2014).
11. Zhang, L. & Hou, Z. *N*-Heterocyclic carbene (NHC)-copper-catalysed transformations of carbon dioxide. *Chem. Sci.* **4**, 3395–3403 (2013).
12. Moore, D. R., Cheng, M., Lobkovsky, E. B. & Coates, G. W. Mechanism of the alternating copolymerization of epoxides and CO₂ Using β-diiminate zinc catalysts: Evidence for a bimetallic epoxide enchainment. *J. Am. Chem. Soc.* **125**, 11911–11924 (2003).
13. Pescarmona, P. P. & Taherimehr, M. Challenges in the catalytic synthesis of cyclic and polymeric carbonates from epoxides and CO₂. *Catal. Sci. Technol.* **2**, 2169–2187 (2012).
14. Anaby, A. *et al.* Bottom-up construction of a CO₂-based cycle for the photocarbonylation of benzene, promoted by a rhodium(I) pincer complex. *J. Am. Chem. Soc.* **138**, 9941–9950 (2016).
15. Li, Y., Sorribes, I., Yan, T., Junge, K. & Beller, M. Selective methylation of amines with carbon dioxide and H₂. *Angew. Chem. Int. Ed.* **52**, 12156–12160 (2013).
16. Angamuthu, R., Byers, P., Lutz, M., Spek, A. L. & Bouwman, E. Electrocatalytic CO₂ conversion to oxalate by a copper complex. *Science* **327**, 313–315 (2010).
17. Costentin, C., Robert, M. & Saveant, J.-M. Catalysis of the electrochemical reduction of carbon dioxide. *Chem. Soc. Rev.* **42**, 2423–2436 (2013).
18. Rosas-Hernández, A., Steinlechner, C., Junge, H. & Beller, M. Photo- and electrochemical valorization of carbon dioxide using earth-abundant molecular catalysts. *Top. Curr. Chem.* **376**, 1 (2017).
19. Wang, W.-H., Himeda, Y., Muckerman, J. T., Manbeck, G. F. & Fujita, E. CO₂ hydrogenation to formate and methanol as an alternative to photo- and electrochemical CO₂ reduction. *Chem. Rev.* **115**, 12936–12973 (2015).
20. Windle, C. D. & Perutz, R. N. Advances in molecular photocatalytic and electrocatalytic CO₂ reduction. *Coord. Chem. Rev.* **256**, 2562–2570 (2012).
21. Berardi, S. *et al.* Molecular artificial photosynthesis. *Chem. Soc. Rev.* **43**, 7501–7519 (2014).
22. Ménard, G. & Stephan, D. W. Room temperature reduction of CO₂ to methanol by Al-based frustrated Lewis pairs and ammonia borane. *J. Am. Chem. Soc.* **132**, 1796–1797 (2010).
23. Barton Cole, E. *et al.* Using a One-electron shuttle for the multielectron reduction of CO₂ to methanol: Kinetic, mechanistic, and structural insights. *J. Am. Chem. Soc.* **132**, 11539–11551 (2010).
24. Wesselbaum, S., vom Stein, T., Klankermayer, J. & Leitner, W. Hydrogenation of carbon dioxide to methanol by using a homogeneous ruthenium–phosphine catalyst. *Angew. Chem. Int. Ed.* **51**, 7499–7502 (2012).

25. Hawecker, J., Lehn, J.-M. & Ziessel, R. Efficient photochemical reduction of CO₂ to CO by visible light irradiation of systems containing Re(bipy)(CO)₃X or Ru(bipy)₃²⁺-Co²⁺ combinations as homogeneous catalysts. *J. Chem. Soc., Chem. Commun.* 536–538, (1983).

26. Morris, A. J., Meyer, G. J. & Fujita, E. Molecular approaches to the photocatalytic reduction of carbon dioxide for solar fuels. *Acc. Chem. Res.* **42**, 1983–1994 (2009).

27. Froehlich, J. D. & Kubiak, C. P. Homogeneous CO₂ reduction by Ni(cyclam) at a glassy carbon electrode. *Inorg. Chem.* **51**, 3932–3934 (2012).

28. Thoi, V. S., Kornienko, N., Margarit, C. G., Yang, P. & Chang, C. J. Visible-light photoredox catalysis: Selective reduction of carbon dioxide to carbon monoxide by a nickel N-heterocyclic carbine-isoquinoline complex. *J. Am. Chem. Soc.* **135**, 14413–14424 (2013).

29. Chen, L. *et al*. Molecular catalysis of the electrochemical and photochemical reduction of CO₂ with earth-abundant metal complexes. Selective production of CO vs HCOOH by switching of the metal center. *J. Am. Chem. Soc.* **137**, 10918–10921 (2015).

30. Chan, S. L.-F., Lam, T. L., Yang, C., Yan, S.-C. & Cheng, N. M. A robust and efficient cobalt molecular catalyst for CO₂ reduction. *Chem. Commun.* **51**, 7799–7801 (2015).

31. Jessop, P. G., Hsiao, Y., Ikariya, T. & Noyori, R. Homogeneous catalysis in supercritical fluids: Hydrogenation of supercritical carbon dioxide to formic acid, alkyl formates, and formamides. *J. Am. Chem. Soc.* **118**, 344–355 (1996).

32. Tanaka, R., Yamashita, M. & Nozaki, K. Catalytic hydrogenation of carbon dioxide using Ir(III)-pincer complexes. *J. Am. Chem. Soc.* **131**, 14168–14169 (2009).

33. Tamaki, Y., Morimoto, T., Koike, K. & Ishitani, O. Photocatalytic CO₂ reduction with high turnover frequency and selectivity of formic acid formation using Ru(II) multinuclear complexes. *Proc. Natl. Acad. Sci. USA* **109**, 15673–15678 (2012).

34. Schmeier, T. J., Dobereiner, G. E., Crabtree, R. H. & Hazari, N. Secondary coordination sphere interactions facilitate the insertion step in an iridium(III) CO₂ reduction catalyst. *J. Am. Chem. Soc.* **133**, 9274–9277 (2011).

35. Langer, R. *et al*. Low-pressure hydrogenation of carbon dioxide catalyzed by an iron pincer complex exhibiting noble metal activity. *Angew. Chem. Int. Ed.* **50**, 9948–9952 (2011).

36. Jiang, Y., Blacque, O., Fox, T. & Berke, H. Catalytic CO₂ activation assisted by rhenium hydride/B(C₆F₅)₃ frustrated Lewis pairs-metal hydrides functioning as FLP bases. *J. Am. Chem. Soc.* **135**, 7751–7760 (2013).

37. Olah, G. A. *et al*. Efficient chemoselective carboxylation of aromatics to arylcarboxylic acids with a superelectrophilically activated carbon dioxide-Al₂Cl₆/Al system. *J. Am. Chem. Soc.* **124**, 11379–11391 (2002).

38. Ohishi, T., Nishiura, M. & Hou, Z. Carboxylation of organoboronic esters catalyzed by N-heterocyclic carbene copper(I) complexes. *Angew. Chem. Int. Ed.* **47**, 5792–5795 (2008).

39. Williams, C. M., Johnson, J. B. & Rovis, T. Nickel-catalyzed reductive carboxylation of styrenes using CO₂. *J. Am. Chem. Soc.* **130**, 14936–14937 (2008).

40. Correa, A. & Martín, R. Palladium-catalyzed direct carboxylation of aryl bromides with carbon dioxide. *J. Am. Chem. Soc.* **131**, 15974–15975 (2009).

41. Yu, D. & Zhang, Y. Copper- and copper-N-heterocyclic carbene-catalyzed C−H activating carboxylation of terminal alkynes with CO₂ at ambient conditions. *Proc. Natl. Acad. Sci. USA* **107**, 20184–20189 (2010).

42. Boogaerts, I. I. F. & Nolan, S. P. Carboxylation of C−H bonds using N-heterocyclic carbene gold(I) complexes. *J. Am. Chem. Soc.* **132**, 8858–8859 (2010).

43. Boogaerts, I. I. F., Fortman, G. C., Furst, M. R. L., Cazin, C. S. J. & Nolan, S. P. Carboxylation of N–H/C–H bonds using N-heterocyclic carbene copper(I) complexes. *Angew. Chem. Int. Ed.* **49**, 8674–8677 (2010).

44. Tsuji, Y. & Fujihara, T. Carbon dioxide as a carbon source in organic transformation: carbon-carbon bond forming reactions by transition-metal catalysts. *Chem. Commun.* **48**, 9956–9964 (2012).

45. Suga, T., Mizuno, H., Takaya, J. & Iwasawa, N. Direct carboxylation of simple arenes with CO₂ through a rhodium-catalyzed C–H bond activation. *Chem. Commun.* **50**, 14360–14363 (2014).

46. Masuda, Y., Ishida, N. & Murakami, M. Light-driven carboxylation of o-alkylphenyl ketones with CO₂. *J. Am. Chem. Soc.* **137**, 14063–14066 (2015).

47. Shimomaki, K., Murata, K., Martin, R. & Iwasawa, N. Visible-light-driven carboxylation of aryl halides by the combined use of palladium and photoredox catalysts. *J. Am. Chem. Soc.* **139**, 9467–9470 (2017).

48. Gui, Y. Y., Zhou, W. J., Ye, J. H. & Yu, D. G. Photochemical carboxylation of activated C(sp₃)−H bonds with CO₂. *ChemSusChem* **10**, 1337–1340 (2017).

49. Ye, J. H. *et al*. Visible-light-driven iron-promoted thiocarboxylation of styrenes and acrylates with CO₂. *Angew. Chem. Int. Ed.* **56**, 15416–15420 (2017).

50. Janes, T., Yang, Y. & Song, D. Chemical reduction of CO₂ facilitated by C-nucleophiles. *Chem. Commun.* **53**, 11390–11398 (2017).

51. Matsumoto, T. *et al*. Nonprecious-metal-assisted photochemical hydrogen production from ortho-phenylenediamine. *J. Am. Chem. Soc.* **135**, 8646–8654 (2013).

52. Carrera, G. V. S. M., da Ponte, M. N. & Branco, L. C. Synthesis and properties of reversible ionic liquids using CO₂, mono- to multiple functionalization. *Tetrahedron* **68**, 7408–7413 (2012).

53. Salvatore, R. N. *et al*. Efficient Cs₂CO₃-promoted solution and solid phase synthesis of carbonates and carbamates in the presence of TBAI. *Tetrahedron* **58**, 3329–3347 (2002).

54. Kamata, K., Kimura, T., Sunaba, H. & Mizuno, N. Scope of chemical fixation of carbon dioxide catalyzed by a bifunctional monomeric tungstate. *Catal. Today* **226**, 160–166 (2014).

55. Kimura, T., Kamata, K. & Mizuno, N. A Bifunctional tungstate catalyst for chemical fixation of CO₂ at atmospheric pressure. *Angew. Chem. Int. Ed.* **51**, 6700–6703 (2012).

56. Yu, B. *et al*. DBU-based ionic-liquid-catalyzed carbonylation of o-phenylenediamines with CO₂ to 2-benzimidazolones under solvent-free conditions. *ACS Catal.* **3**, 2076–2082 (2013).

57. Schmidt, A., Shilabin, A. G. & Nieger, M. On benzo[*b*][1,4]diazepinium-olates, -thiolates and -carboxylates as anti-Hückel mesomeric betaines. *Org. Biomol. Chem.* **1**, 4342–4350 (2003).

58. Hansen, M. *et al*. Synthesis and pharmacological evaluation of N-benzyl substituted 4-bromo-2,5-dimethoxyphenethylamines as 5-HT₂A/2C partial agonists. *Biorg. Med. Chem.* **23**, 3933–3937 (2015).

59. Weller, H. & Grellmann, K. H. On the photochemical synthesis of N,N′-dimethylindolo[2,3-*c*] carbazole and the mechanism of its formation from N,N′-dimethyl-N,N′-diphenyl-1,4-phenylenediamine. *J. Am. Chem. Soc.* **105**, 6268–6273 (1983).

60. Ngo, T. H. A., Tran, D. T. & Dinh, C. H. Surface photochemical graft polymerization of acrylic acid onto polyamide thin film composite membranes. *J. Appl. Polym. Sci.* **134**, 44418 (2017).

61. Mei, L. *et al*. Synthesis and catalytic activity of novel Zn-N and Cu-N complexes. *Inorg. Chem. Commun.* **13**, 1009–1013 (2010).

62. Adams, C. J., Haddow, M. F., Lusi, M. & Orpen, A. G. Crystal synthesis of 1,4-phenylenediamine salts and coordination networks. *Cryst Eng Comm* **13**, 4324–4331 (2011).

63. Wakizaka, M., Matsumoto, T., Tanaka, R. & Chang, H.-C. Dehydrogenation of anhydrous methanol at room temperature by o-aminophenol-based photocatalysts. *Nat. Commun.* **7**, 12333 (2016).

64. Büttner, T. *et al*. A stable aminyl radical metal complex. *Science* **307**, 235–238 (2005).

65. Xu, M., Jupp, A. R. & Stephan, D. W. Stoichiometric reactions of CO₂ and indium-silylamides and catalytic synthesis of ureas. *Angew. Chem. Int. Ed.* **56**, 14277–14281 (2017).

66. Morgenstern, D. A., Wittrig, R. E., Fanwick, P. E. & Kubiak, C. P. Photoreduction of carbon dioxide to its radical anion by nickel cluster [Ni$_3$(μ^3-I)$_2$(dppm)$_3$]: Formation of two carbon-carbon bonds *via* addition of carbon dioxide radical anion to cyclohexene. *J. Am. Chem. Soc.* **115**, 6470–6471 (1993).

67. Xiong, T. & Zhang, Q. New amination strategies based on nitrogen-centered radical chemistry. *Chem. Soc. Rev.* **45**, 3069–3087 (2016).

68. Kaim, W. Manifestations of noninnocent ligand behavior. *Inorg. Chem.* **50**, 9752–9765 (2011).

69. Suarez, A. I. O., Lyaskovskyy, V., Reek, J. N. H., van der Vlugt, J. I. & de Bruin, B. Complexes with nitrogen-centered radical ligands: Classification, spectroscopic features, reactivity, and catalytic applications. *Angew. Chem. Int. Ed.* **52**, 12510–12529 (2013).

70. Hicks, R. G. Metal Complexes of aminyl radicals. *Angew. Chem. Int. Ed.* **47**, 7393–7395 (2008).

71. Merényi, G. & Lind, J. In *N-Centered Radicals*, Alsfassi, Z. Ed. Wiley, New York, 599–613 1998.

Acknowledgements

Author Contributions

Experimental data were collected by D.U., R.N., and T.K. The manuscript was written by T.M. and H.-C.C. conceived and directed the project.

Additional Information

Supplementary information accompanies this paper at https://doi.org/10.1038/s41598-018-33060-3.

Competing Interests: The authors declare no competing interests.

Publisher's note: Springer Nature remains neutral with regard to jurisdictional claims in published maps and institutional affiliations.